physica status solidi rrl
www.pss-rapid.com

Laser- and Ion-Induced Defect Engineering in WS_2 Monolayers

Aswin Asaithambi, Roland Kozubek, Günther M. Prinz, Francesco Reale, Erik Pollmann, Marcel Ney, Cecilia Mattevi, Marika Schleberger,* and Axel Lorke**

Tungsten disulfide is one of the prominent transition metal dichalcogenide materials, which shows a transition from an indirect to a direct bandgap as the layer thickness is reduced down to a monolayer. To use WS_2 monolayers in devices, detailed knowledge about the luminescence properties regarding not only the excitonic but also the defect-induced contributions is needed. Herein, WS_2 monolayers are irradiated with Xe^{30+} ions with different fluences to create different defect densities. Apart from the excitonic contributions, two additional emission bands are observed at low temperatures. These bands can be reduced or even suppressed, if the flakes are exposed to laser light with powers up to 1.5 mW. Increasing the temperature up to room temperature leads to recovery of this emission, so that the luminescence properties can be modified using laser excitation and temperature. The defect bands emerging after ion irradiation are attributed to vacancy defects together with physisorbed adsorbates at different defect sites.

2D monolayers of transition metal dichalcogenides (TMDCs) have drawn much interest in recent times due to their excellent physical properties such as indirect to direct bandgap transition (with bandgap energies mostly in the visible and near-infrared region) when going from bulk to monolayer thickness.[1,2] This makes them attractive for optoelectronic device applications.[3–5] TMDCs also show excellent spin–orbit coupling (control over polarization-dependent band excitation), mobility, and strong exciton binding energies.[6–10] WS_2 monolayers show higher luminescence quantum yield (≈6%) when compared with other TMDC monolayers (<1%).[11] Also, the formation of quantum emitters (e.g., for quantum information processing) at defects or at specific positions defined by strain engineering has been reported.[12–16] Although it has been over a decade since the discovery of graphene and 2D materials, practical applications of these 2D materials have not lived up to the expectation. The main reason, apart from the growth and fabrication, of which significant improvements have already been realized, is the defect-prone nature of these materials.

To realize the potential of 2D TMDCs in various applications, defects in these materials must be better understood. Raman spectroscopy has proved to be a valuable tool to characterize graphene monolayers, where, e.g., the intensity ratio of D and G band peaks is used to nondestructively study defects in this material.[17,18] For TMDCs, however, no direct correlation between Raman spectroscopy and defect structure has been found. Photoluminescence (PL) spectroscopy at low temperature (LT), where defect-bound excitons can recombine radiatively, has proven to be a promising nondestructive technique to characterize defects in TMDC monolayers.[19–22] Using higher excitation powers and temperature variations it is possible to change the luminescence emission of the TMDC monolayers and to reveal the nature of the underlying defect.[19,23] He et al. reported that exposure of aged WS_2 monolayers to higher excitation power at cryogenic temperature led to the observation of a new defect-bound emission.[19] Lu et al. reported that oxygen substitution in the chalcogen vacancy defects heals the defect band and thereby increases the conductivity of the TMDC monolayers.[24] At the same time, defects can also induce local confinement of the charge carriers and subsequently, single photon emission from these confined regions was observed. Therefore, it is imperative to study the defects in the TMDC monolayers for understanding both how to exploit them and to find efficient ways to anneal them.

In this report we studied chemical vapor deposition (CVD)-grown WS_2 monolayers irradiated with Xe^{30+} ions using μ-PL spectroscopy at different excitation powers and temperature cycles to get a deeper insight into possible defect natures and to actively change the luminescence properties of the material.

Figure 1 shows PL spectra from an as-synthesized WS_2 monolayer at room temperature (RT) and 83 K. The RT spectrum shows mainly one asymmetric line at ≈630 nm. The line is broadened to higher wavelengths, which was already reported

Dr. A. Asaithambi, Dr. R. Kozubek, Dr. G. M. Prinz, E. Pollmann, M. Ney, Prof. M. Schleberger, Prof. A. Lorke
Fakultät für Physik and CENIDE
Universität Duisburg-Essen
D-47048 Duisburg, Germany
E-mail: aswinfb@gmail.com; marika.schleberger@uni-due.de; axel.lorke@uni-due.de

Dr. F. Reale, Dr. C. Mattevi
Department of Materials
Imperial College
London SW7 2AZ, UK

The ORCID identification number(s) for the author(s) of this article can be found under https://doi.org/10.1002/pssr.202000466.

DOI: 10.1002/pssr.202000466

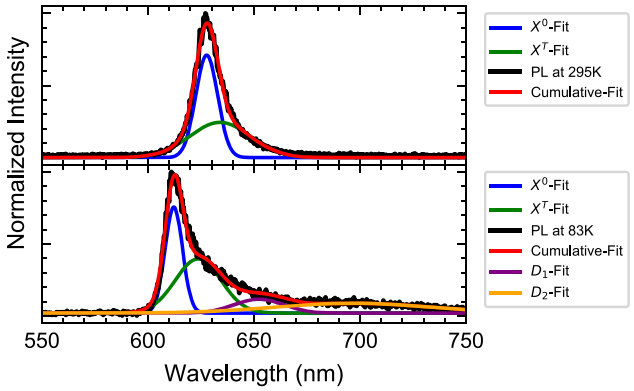

Figure 1. PL spectra (excitation power = 0.5 μW) at RT (upper panel) and 83 K (lower panel) of WS_2 monolayers on SiO_2/Si substrate. The excitonic line shows an asymmetry to higher wavelengths ascribed to an unresolved combination of free exciton and trion emission. The red and green curves are best fits for the two contributions, respectively. The purple and orange line fits correspond to two defect-bound emissions.

in the literature and is accordingly ascribed to an unresolved combination of free exciton (X^0) and trion (X^T) emission.[20,22,25] The LT spectrum also mainly shows this excitonic emission, which is shifted to ≈610 nm because lowering the temperature leads to a widening of the bandgap.[23] No further strong contributions, often observed in LT spectra of WS_2 monolayers at higher wavelengths, which are usually ascribed to defect or degradation-induced luminescence,[19–22] have been observed for these as-synthesized WS_2 monolayers. Only a very small hump around 650 and 700 nm can be seen. This observation suggests that these CVD-grown flakes were almost free of defects or aging-induced deterioration, making them perfectly suited for this study on defect engineering.

Figure 2a shows an intensity map of the exciton emission intensity (indicated by the red line in Figure 2d) of a single flake of an as-synthesized WS_2 monolayer at RT. A distinct pattern in the exciton emission intensity is found within a single flake. Three distinct triangles were observed either from the intensity map or from the wavelength map (Figure 2b). These three triangles are separated by darker lines (lower emission) in Figure 2a and a blueshifted emission in Figure 2b. Such a behavior was already observed by other groups and attributed to inner grain boundaries and material heterogeneity formed during the growth of WS_2 monolayers (see, e.g., ref. [15,20], and references therein).[20,26] To highlight the good quality of the sample, Figure 2b shows the map of exciton peak wavelength (λ_{max}) (indicated by the green line in Figure 2d) from the flake. Only

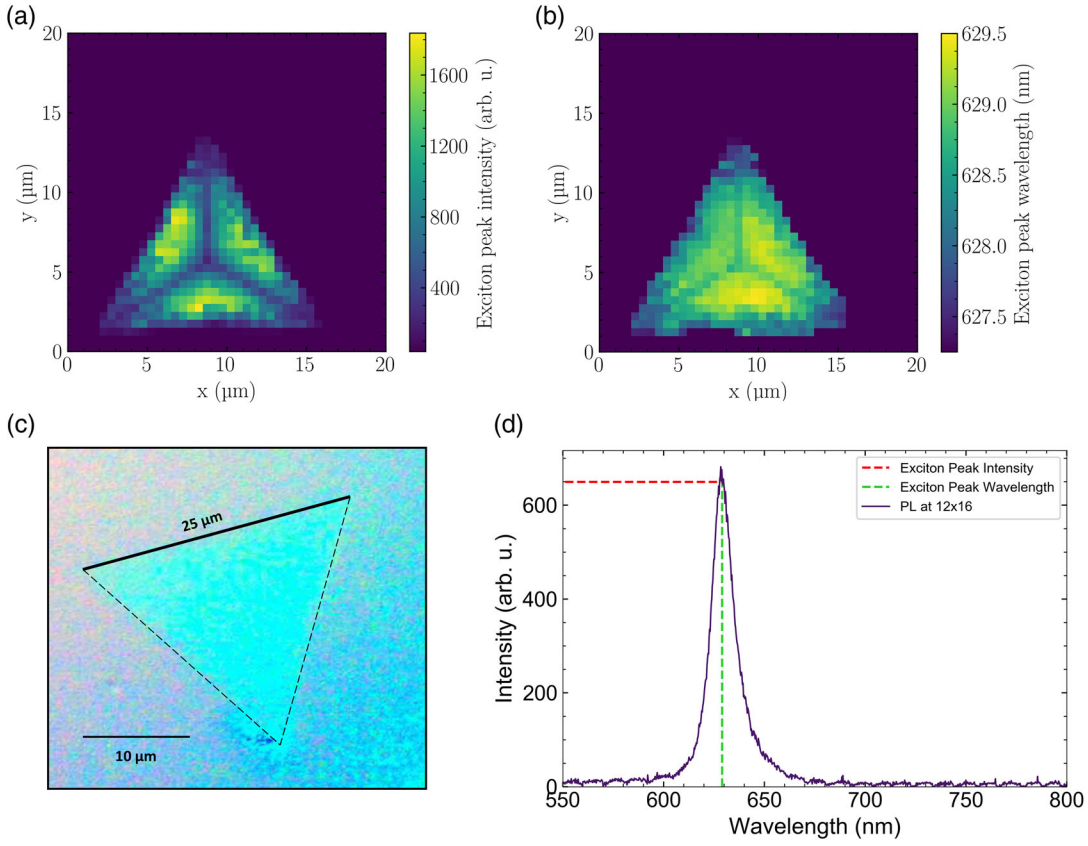

Figure 2. a) PL map (excitation power = 25 μW) of the intensity at RT of a WS_2 monolayer. Darker lines exhibiting lower emission divide the flake into three subtriangles. b) Map of the wavelength at maximum emission. Variations are only very small up to 2 nm across the flake. The threefold structure is also seen here. c) Optical microscopy image of a single flake (color enhanced for clarity), showing just one homogenous triangle. d) PL spectrum from one point of the map.

a very small fluctuation of $\Delta\lambda_{max} < 2$ nm is found within the flake. The observed homogeneity for our sample in the emission wavelength at maximum intensity indicates the absence of large variations of strain in the flake and strong band renormalization due to free charge carriers.[20] From RT PL map, we can further confirm the good quality of the pristine WS_2 monolayers. Low-temperature excitation power-dependent measurements (Figure S1, Supporting Information) on pristine sample showed only the exciton contribution and did not show any laser-induced changes which further confirms the good quality of the pristine WS_2 monolayers.

Figure 3 shows LT-PL spectra of the sample irradiated with Xe^{30+} ions of the following fluences: 500, 1500, 2500, 3500, 4500, and 6000 μm^{-2}. For this purpose, we used a metal mask with nine holes (see Figure S2, Supporting Information) in it through which the underlying WS_2 monolayers on Si/SiO_2 substrate were irradiated with Xe^{30+} ions in different fluences. Three holes were left unirradiated to study defect-related emission caused by aging. The overall PL intensity is decreasing with increasing ion fluence, as it is expected for samples with increasing defect density (see Figure S3, Supporting Information). After irradiating the monolayer flakes with the Xe^{30+} ions, we observe mainly the appearance of two new emission bands apart from the excitonic contribution. The first one at ≈650 nm (D_1) and a second one at ≈720 nm (D_2). These two contributions vary in intensity not only with increasing ion fluence, but also slightly within the same flake. Note that the exciton peak position remains the same for the WS_2 flakes irradiated with different fluences of Xe^{30+} ions, indicating that the bandgap of the material is not affected by the ion irradiation.

For low ion fluences, D_2 dominates the spectrum but for higher fluences, D_1 is the dominating contribution. Only the flake irradiated with 3500 μm^{-2} Xe^{30+} ion fluence is an outlier that does not follow these trends. For all ion fluences, we still observe the excitonic emission peak at 610 nm even for the most damaged flakes. Surprisingly, flakes, that are irradiated with higher Xe^{30+} ion fluences, exhibit a stronger excitonic contribution in relation to the D_1 and D_2 emission bands compared with monolayers irradiated with lower ion fluences. Based on these observations, we suppose that the D_2 emission band is more likely due to isolated defect sites, while the D_1 emission band, showing up more pronounced at higher defect densities, is due to defect complexes like, e.g., double vacancies or line defects. If the fluences are further increased, nonradiative defect complexes are formed with higher and higher percentage, leading to an overall reduced intensity but with a larger exciton-to-defect emission ratio compared with the less irradiated monolayers.

As a next step, to get a deeper insight into these two bands, we conducted a power-dependent laser excitation process while simultaneously measuring PL. For this purpose, we started with a laser power of 0.5 μW and increased it to 10, 50, 100, 300, 700, and 1500 μW. After that we reduced the excitation power in the same steps again. Selected PL spectra for the monolayers irradiated with 1500 ions μm^{-2} are shown in **Figure 4**. With increasing excitation power (red lines), the two emission bands D_1 and D_2 decrease in intensity compared with the excitonic contribution at ≈610 nm. As expected, the intensity of the excitonic emission increases linearly with laser power (see Figure S4, Supporting Information), while the D_1 and D_2 emission bands show a sublinear behavior. In addition, the defect lines show a shift to lower wavelengths with increasing power (see Figure S5, Supporting Information), while the exciton line stays at a constant

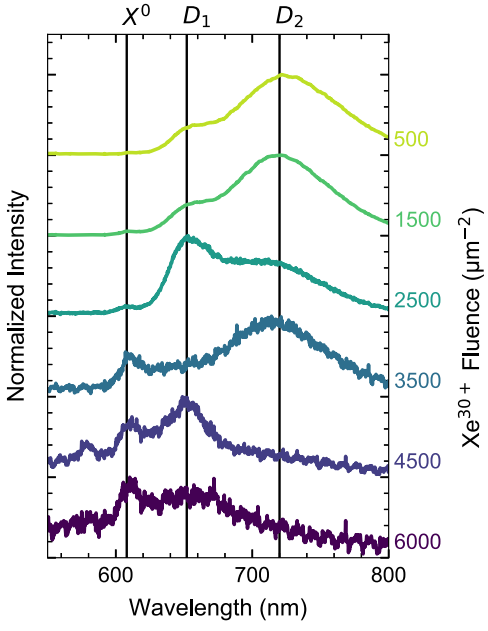

Figure 3. LT normalized PL spectra of WS_2 monolayers, irradiated with different fluences of Xe^{30+} ions. The two bands D_1 and D_2 related to defects are always observable in different intensities apart from the excitonic contribution. The spectra are shifted for better clarity.

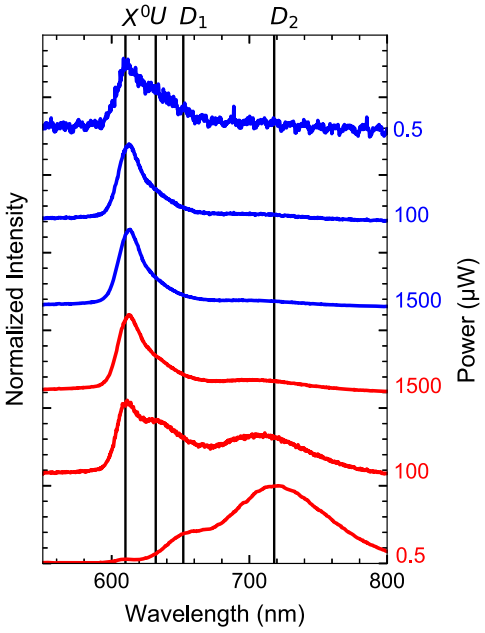

Figure 4. PL spectra at different excitation powers of a WS_2 monolayer irradiated with 1500 μm^{-2} fluence of Xe^{30+} at 83 K. The red curves were taken while increasing the excitation power and the blue curves while decreasing the excitation power again. A shift and suppression of the D_1 and D_2 bands can be observed. The spectra are shifted for better clarity.

wavelength at low excitation power. At high excitation power, more emission contribution from trion is observed, which leads to a small redshift of the exciton emission.[27,28] After reducing the power again, D_1 and D_2 remain almost completely absent. On the higher wavelength side of the excitonic contribution, another emission band at ≈630 nm has formed. It is about 60 meV separated from the free exciton emission. A peak in the same wavelength range was also found by He et al (called "U" peak in their publication) after a similar laser treatment of their samples.[19] They found this peak only for aged samples and proposed it to be helpful identifying aged samples. This is not applicable for our WS_2 monolayer flakes because—as we have already pointed out earlier—our sample did not show a pronounced emission band below the excitonic emission before irradiation with ions which could be related to aging or deterioration (bottom panel in Figure 1).

The intensity of the excitonic contribution after such a laser process of irradiated monolayers is almost the same as for the very first measurement at 0.5 μW (shown in Figure S6, Supporting Information). This observation leads us to conclude that the material quality itself is not enhanced by this laser process. Therefore, the question arises, whether this transformation in the emission properties of the differently irradiated WS_2 monolayer flakes induced by the laser excitation is persistent.

To check the persistence of the laser processing effect, we performed temperature cycle experiments and the results are shown in **Figure 5**. Figure 5 shows five different PL spectra at LT with 0.5 μW excitation power for a flake irradiated with 1500 μm^{-2} Xe^{30+} ion fluence. Figure 5a shows the spectrum of the as-irradiated monolayer where D_1 and D_2 dominate the spectrum. When a laser processing step (ramping up and down the laser power) is performed, D_1 and D_2 vanish and only the exciton contribution is observed as shown in Figure 5b (see also Figure 4). After the sample was slowly warmed up to RT under vacuum and cooled back to 83 K, the spectrum shows the reappearance of the defect-bound emissions, where D_1 exhibits a stronger recovery than D_2 (see Figure 5c). This clearly shows that the laser processing is not persistent. To check if this recovered defect-bound emissions can be suppressed again, a second laser processing step was performed. The resulting spectrum shows again the disappearance of both D_1 and D_2, as shown in Figure 5d. This demonstrated that the laser processing is non-permanent but reproducible. Finally, the sample was warmed up to RT and exposed to ambient air. The sample was cooled back to 83 K and, lastly, the spectrum shown in Figure 5e was recorded. It shows the recovery of the defect-bound emissions similar to that of Figure 5c.

These observations lead to the following conclusions. First, the PL variations induced by the laser processing is not persistent, as it was also reported from He et al. for the "U" peak,[19] but they are reproducible. Second, after a laser processing step and a temperature cycle, D_1 and D_2 have recovered, from which we conclude that physisorbed molecules linked to defect sites are responsible for the observed changes in the luminescence properties. By ramping up the laser power, during the laser processing step, the molecules desorb from the defect sites and D_1 and D_2 vanish. A temperature increase in the whole sample to RT in vacuum or in air leads to a redecoration of the defect sites with molecules still attached to the sample surface or coming from the fresh air. This results in a recovery of D_1 and D_2. A more detailed view shows that the intensity ratio of the recovered D_1 and D_2 emission (Figure 5c or 5e) compared with the as-grown situation (Figure 5a) is different. The D_2 emission recovers weaker than D_1. This behavior can be explained if a certain part of the defect

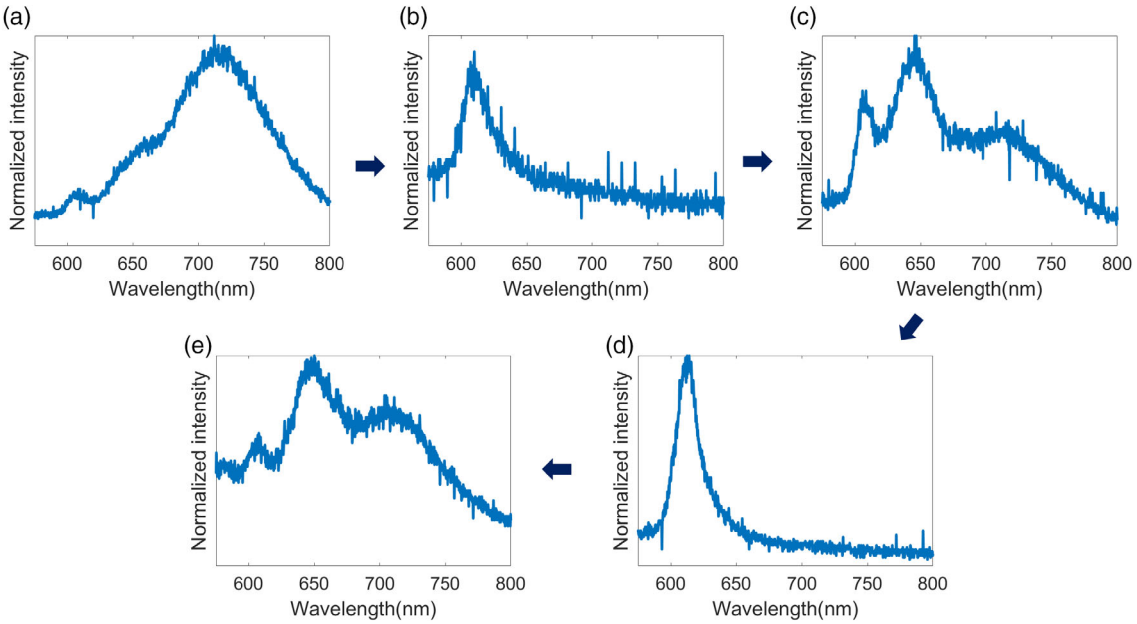

Figure 5. a–e) PL spectra at 83 K with 0.5 μW excitation power of a WS_2 monolayer irradiated with 1500 μm^{-2} fluence of Xe^{30+} ions at different annealing steps: a) as-irradiated, b) after first laser processing, c) after one temperature cycle (83 K to RT and back to 83 K under constant vacuum), d) after second laser processing, e) after another temperature cycle with additionally purging the cryostat with air at RT. The emission bands D_1 and D_2 are recovering, if the temperature is increased to RT.

sites responsible for the D_2 emission gets transformed into other defect types by laser exposure. Such a transformation was observed, e.g., for sulfur vacancies mobilized by electron beam irradiation.[29] Komsa et al. observed that isolated vacancies form line defects during the e-beam irradiation.[29] For isolated sulfur vacancies, an energy barrier of 2.3 eV was calculated for MoS_2 monolayers, which is drastically lowered for neighboring vacancies to about 0.8 eV.[29] These hopping barriers might also be overcome by the laser exposure, leading to a rearrangement of sulfur vacancies, assuming that the hopping barrier is of similar energy and behavior for WS_2 monolayers. When unirradiated, but aged, flakes were subjected to the laser excitation process but now directly at RT followed by collecting LT-PL (Figure S7, Supporting Information), D_2 was found to be almost absent; only the D_1 and X^0 emission persisted. This further strengthens our argument of an evolution of ion-induced or aging-related isolated defects into more complex defect structures as a result of laser and temperature processing.

Ion irradiation is a well-known tool to introduce defects into 2D materials.[30] The exact nature of the defects depends on the specific ion beam parameters and the respective 2D material. While it is often extremely difficult to conclude on the defect type by spectroscopic methods, it can, in principle, be determined by scanning transmission electron microscopy (STEM). However, this requires freestanding samples and the substrate has a large influence on the defect type as well. As a rule of thumb, single vacancies are the most likely defect if ions in the nuclear stopping regime are used.[31,32] In this work, we use highly charged ions (HCIs) which in addition to the defect creation by nuclear collisions (corresponding to the kinetic energy of the ion of 180 keV) may create defects due to the direct excitation of the electronic system (corresponding to the potential energy of the ion of 15 keV). The latter should enhance the probability to create more complex defects like double vacancies, for instance. Furthermore, the spatial extension of the defective area created by an individual ion is typically larger for HCIs than for singly charged ions and can be controlled by varying the charge state.[33,34]

By the irradiation of our samples with Xe^{30+}, it is thus very likely that sulfur vacancies are created. These will appear predominantly not only as single vacancies but also as divacancies or even more complex forms because electronic excitation of the target material is to be expected. Kastl et al. reported an emission band at 710 nm at LT and could correlate it to regions with a sulfur deficiency of 10%.[20] Carozo et al. also found a similar relation between PL emission lines and regions with monosulfur vacancies.[21] Comparison of the spectral position of D_2 with theoretical and experimental data from the literature suggests that the D_2 emission originates from bare isolated sulfur vacancies forming a stable intergap state.[35,36] But this assignment cannot explain our measurements and findings from other groups. This is first that after a laser processing step the D_2 emission vanishes, which is not expected for bare sulfur vacancies, where intergap states are formed.[37] Our suggestion is therefore that adsorbates bind to oxygen-substituted sulfur vacancies forming emissive states within the bandgap and are responsible for the D_2 emission. Barja et al. showed that bare oxygen-substituted sulfur vacancies are easily formed and do not lead to an intergap state.[37] This means that after a desorption of molecules, due to the rising laser power, the emission also vanishes, as observed in our experiment. Second, after a temperature cycle (ramping up and down the sample temperature in vacuum or in air) the emission recovers, which could be due to a redecoration of the oxygen substituted sulfur vacancies with molecules, also explainable by our suggestion. This assumption can be further substantiated by the LT-PL map of an aged WS_2 monolayer flake (see Figure S8, Supporting Information), where the D_2/D_1 intensity ratio is higher at the edge than at the middle of the flake. As mentioned before, Kastl et al. reported that single sulfur defects are found predominantly at the edges of the flakes, where they also found a LT-PL emission at 710 nm, so in the same region as the D_2 emission, observed by us. Therefore, with great certainty, based on the observation from the LT-PL map, LT and RT laser processing, and comparison with the literature, we suggest that decorated simple vacancy defects possibly substituted with oxygen are responsible for the D_2 emission. In addition, this assumption can also explain that for a low ion irradiation fluence D_2 is dominating the PL spectra (see Figure 3), while for higher ion fluences D_1 is starting to dominate. This is expected because as higher the irradiation fluence gets, the higher is the probability to form more complex defects instead of single sulfur vacancies. For the D_1 emission we tentatively propose a similar origin, where a more complex defect like, e.g., a double vacancy or a line defect decorated with physisorbed molecules leads to a similar luminescence behavior during laser processing and temperature cycling like for the D_2 emission. Also, tungsten vacancies might play a role in this process. From the literature it is known that these defects tend to either heal themselves very fast, because of the tungsten ions, which are only shifted to nearby positions and come back again, or form nanopores or larger defects like holes.[38] Therefore, we propose that isolated tungsten vacancies do not play a major role in our laser excitation process, even if they are also formed by the Xe^{30+} ion irradiation. Also, for this type of defect intergap states are expected.[35,36] These results show that the optical properties of the WS_2 monolayers can be engineered either persistently using, e.g., Xe^{30+} ion irradiation or reversibly using laser excitation and temperature cycling. The observation of defect luminescence, that is related to physisorbed molecules, might be very interesting for sensing applications which would also allow to reset the sensor by just using a noncontact optical excitation step.

In conclusion, we have performed power- and temperature-dependent PL measurements of pristine and Xe^{30+} ion irradiated WS_2 monolayer flakes to systematically create and engineer defects. After irradiation we observe defect-related emission bands at LT for all monolayer flakes. The intensity of these emission bands depends not only on the ion fluence but also on the laser treatment of the sample. Using power-dependent laser excitation, we induced a change in the optical properties of the monolayers. We observe a decreasing intensity together with a shift to shorter wavelengths for the defect-related emission bands D_1 and D_2, while the near bandgap emission stays at its original position during the laser excitation. After a temperature cycle to RT and to LT again, we observe that the defect-related emission bands D_1 and D_2 reappear. Because of this behavior we assign the D_2 emission band to adsorbate-decorated single sulfur vacancies created by nuclear stopping which can be substituted with oxygen. The emission band D_1 is presumed to originate from adsorbate-decorated defect complexes like, e.g., double vacancies or line defects

stemming from the energy deposition by electronic excitation. Using laser processing, we desorb the physisorbed adsorbates and partially transform the defect type created by the ion irradiation, but we do not improve the material quality of the WS_2 monolayer flakes, as indicated by the near bandgap emission, which does not show an increase in intensity after laser processing.

Experimental Section

WS_2 flakes were synthesized via CVD technique using a hot-wall quartz tube furnace.H_2WO_4 (0.2 g) (Sigma, 99.99%) mixed with 0.2 g of NaCl (Sigma, 99.99%) was placed in an alumina boat in the center of the tubular furnace, whereas 0.6 g of S powder (Sigma, 99.99%) was placed in another boat in the upstream region, controlled independently with another heating module. The substrate was Si/SiO_2, cleaned by ultrasonication in deionized water, acetone, and isopropanol and placed close to the W-containing boat in the downstream direction. The reactor was purged with 200 sccm of high purity argon gas for 30 min at 200 °C. Afterward the furnace was heated up to 850 °C at 25 °C min^{-1}. In the meantime, the S boat was heated up to 125 °C at 5 °C min^{-1} using 100 sccm of Ar. These temperatures were kept for 15 min and then the furnace was naturally cooled down.[39] After a first PL characterization of the pristine monolayers, the monolayer flakes were irradiated with different fluences of Xe^{30+} ions. The irradiation process was performed at the Highly Charged Ion Collisions with Surfaces (HICS) beamline at the University of Duisburg-Essen updated with an electron-beam ion source (EBIS).[40] This source can be used to deliver highly charged xenon ions with high potential energy, which have been shown to introduce defects in 2D materials in a controlled way.[41] To study the PL dependency on the defect density, six different spots on the sample were irradiated perpendicularly with Xe^{30+} ions with kinetic energy of 180 keV and different fluences ranging from 500 to 6000 ions μm^{-2} (see Figure S1, Supporting Information). The PL measurements were carried out in a custom-built μ-PL setup. This setup consists of a 532 nm solid state laser for excitation and a spectrometer with 0.5 m focal length, equipped with a 150 mm^{-1} grating and a liquid nitrogen cooled CCD camera for analyzing the emitted light. The excitation laser is focused onto the sample with a 50× microscope objective, reaching a spot size of ≈1–2 μm. To record PL at LT, we use a continuous flow cryostat, with which we reach temperatures down to 83 K using liquid nitrogen as cooling agent. The pressure inside the cryostat was maintained at 8×10^{-6} mbar for all LT measurements.

Supporting Information

Supporting Information is available from the Wiley Online Library or from the author.

Acknowledgements

A.A. acknowledges IMPRS-SurMat for the Ph.D. scholarship. C.M. thanks the award of a Royal Society University Research Fellowship by the UK. Royal Society; EPSRC Grant No. EP/M022250/1; and EPSRC-Royal Society Fellowship Engagement Grant No. EP/L003481/1. R.K., E.P., and M.S. acknowledge support from the DFG by funding SCHL 384/20-1 (project number 406 129 719). Open access funding enabled and organized by Projekt DEAL.

Conflict of Interest

The authors declare no conflict of interest.

Keywords

defects, ion irradiation, laser annealing, photoluminescence, transition metal dichalcogenides, WS_2

Received: September 24, 2020
Revised: October 13, 2020
Published online: November 23, 2020

[1] A. Splendiani, L. Sun, Y. Zhang, T. Li, J. Kim, C.-Y. Chim, G. Galli, F. Wang, *Nano Lett.* **2010**, *10*, 1271.
[2] K. F. Mak, C. Lee, J. Hone, J. Shan, T. F. Heinz, *Phys. Rev. Lett.* **2010**, *105*, 136805.
[3] D. Andrzejewski, E. Hopmann, M. John, T. Kuemmell, G. Bacher, *Nanoscale* **2019**, *11*, 8372.
[4] Q. Zeng, Z. Liu, *Adv. Electron. Mater.* **2018**, *4*, 1700335.
[5] D. Andrzejewski, H. Myja, M. Heuken, A. Grundmann, H. Kalisch, A. Vescan, T. Kammell, G. Bacher, *ACS Photonics* **2019**, *6*, 1832.
[6] D. Xiao, G.-B. Liu, W. Feng, X. Xu, W. Yao, *Phys. Rev. Lett.* **2012**, *108*, 19.
[7] B. Zhu, X. Chen, X. Cui, *Sci. Rep.* **2015**, *5*, 9218.
[8] S. Park, N. Mutz, T. Schultz, S. Blumstengel, A. Han, A. Aljarb, L.-J. Li, E. J. W. List-Kratochvil, P. Amsalem, N. Koch, *2D Mater.* **2018**, *5*, 025003.
[9] Z. Yu, Z.-Y. Ong, S. Li, J.-B. Xu, G. Zhang, Y.-W. Zhang, Y. Shi, X. Wang, *Adv. Funct. Mater.* **2017**, *27*, 1604093.
[10] S. H. Mir, V. K. Yadav, J. K. Singh, *ACS Omega* **2020**, *5*, 14203.
[11] L. Yuan, L. Huang, *Nanoscale* **2015**, *7*, 7402.
[12] C. Chakraborty, L. Kinnischtzke, K. M. Goodfellow, R. Beams, A. N. Vamivakas, *Nat. Nanotechnol.* **2015**, *10*, 507.
[13] Y.-M. He, G. Clark, J. R. Schaibley, Y. He, M.-C. Chen, Y.-J. Wei, X. Ding, Q. Zhang, W. Yao, X. Xu, C.-Y. Lu, J.-W. Pan, *Nat. Nanotechnol.* **2015**, *10*, 497.
[14] M. Koperski, K. Nogajewski, A. Arora, V. Cherkez, P. Mallet, J.-Y. Veuillen, J. Marcus, P. Kossacki, M. Potemski, *Nat. Nanotechnol.* **2015**, *10*, 503.
[15] A. Srivastava, M. Sidler, A. V. Allain, D. S. Lembke, A. Kis, A. Imamoğlu, *Nat. Nanotechnol.* **2015**, *10*, 491.
[16] J. Kern, I. Niehues, P. Tonndorf, R. Schmidt, D. Wigger, R. Schneider, T. Stiehm, S. M. de Vasconcellos, D. E. Reiter, T. Kuhn, R. Bratschitsch, *Adv. Mater.* **2016**, *28*, 7101.
[17] A. C. Ferrari, D. M. Basko, *Nat. Nanotechnol.* **2013**, *8*, 235.
[18] A. Eckmann, A. Felten, A. Mishchenko, L. Britnell, R. Krupke, K. S. Novoselov, C. Casiraghi, *Nano Lett.* **2012**, *12*, 3925.
[19] Z. He, X. Wang, W. Xu, Y. Zhou, Y. Sheng, Y. Rong, J. M. Smith, J. H. Warner, *ACS Nano* **2016**, *10*, 5847.
[20] C. Kastl, R. J. Koch, C. T. Chen, J. Eichhorn, S. Ulstrup, A. Bostwick, C. Jozwiak, T. R. Kuykendall, N. J. Borys, F. M. Toma, S. Aloni, A. Weber-Bargioni, E. Rotenberg, A. M. Schwartzberg, *ACS Nano* **2019**, *13*, 1284.
[21] V. Carozo, Y. Wang, K. Fujisawa, B. R. Carvalho, A. McCreary, S. Feng, Z. Lin, C. Zhou, N. Perea-López, A. L. Elas, B. Kabius, V. H. Crespi, M. Terrones, *Sci. Adv.* **2017**, *3*, e1602813.
[22] P. K. Chow, R. B. Jacobs-Gedrim, J. Gao, T.-M. Lu, B. Yu, H. Terrones, N. Koratkar, *ACS Nano* **2015**, *9*, 1520.
[23] R. Kaupmees, M. Grossberg, M. Ney, A. Asaithambi, A. Lorke, J. Krustok, *Phys. Status Solidi RRL* **2019**, *14*, 1900355.
[24] J. Lu, A. Carvalho, X. K. Chan, H. Liu, B. Liu, E. S. Tok, K. P. Loh, A. H. C. Neto, C. H. Sow, *Nano Lett.* **2015**, *15*, 3524.
[25] G. Plechinger, P. Nagler, A. Arora, R. Schmidt, A. Chernikov, A. G. del Águila, P. C. Christianen, R. Bratschitsch, C. Schueller, T. Korn, *Nat. Commun.* **2016**, *7*, 12715.

[26] H. Liu, J. Lu, K. Ho, Z. Hu, Z. Dang, A. Carvalho, H. R. Tan, E. S. Tok, C. H. Sow, *Nano Lett.* **2016**, *16*, 5559.
[27] K. Wei, Y. Liu, H. Yang, X. Cheng, T. Jiang, *Appl. Opt.* **2016**, *55*, 6251.
[28] A. O. A. Tanoh, J. Alexander-Webber, J. Xiao, G. Delport, C. A. Williams, H. Bretscher, N. Gauriot, J. Allardice, R. Pandya, Y. Fan, Z. Li, S. Vignolini, S. D. Stranks, S. Hofmann, A. Rao, *Nano Lett.* **2019**, *19*, 6299.
[29] H.-P. Komsa, S. Kurasch, O. Lehtinen, U. Kaiser, A. V. Krasheninnikov, *Phys. Rev. B* **2013**, *88*, 035301.
[30] M. Schleberger, J. Kotakoski, *Materials* **2018**, *11*, 1885.
[31] O. Lehtinen, J. Kotakoski, A. V. Krasheninnikov, A. Tolvanen, K. Nordlund, J. Keinonen, *Phys. Rev. B* **2010**, *81*, 153401.
[32] S. Kretschmer, M. Maslov, S. Ghaderzadeh, M. Ghorbani-Asl, G. Hlawacek, A. V. Krasheninnikov, *ACS Appl. Mater. Interfaces* **2018**, *10*, 30827.
[33] J. Hopster, R. Kozubek, B. Ban-d'Etat, S. Guillous, H. Lebius, M. Schleberger, *2D Mater.* **2014**, *1*, 011011.
[34] R. Kozubek, P. Ernst, C. Herbig, T. Michely, M. Schleberger, *ACS Appl. Nano Mater.* **2018**, *1*, 3765.
[35] S. Salehi, A. Saffarzadeh, *Surf. Sci.* **2016**, *651* 215.
[36] X. Zhao, X. Dai, C. Xia, T. Wang, *Superlattice Microstruct.* **2015**, *85*, 339.
[37] S. Barja, S. Refaely-Abramson, B. Schuler, D. Y. Qiu, A. Pulkin, S. Wickenburg, H. Ryu, M. M. Ugeda, C. Kastl, C. Chen, C. Hwang, A. Schwartzberg, S. Aloni, S.-K. Mo, D. F. Ogletree, M. F. Crommie, O. V. Yazyev, S. G. Louie, J. B. Neaton, A. Weber-Bargioni, *Nat. Commun.* **2019**, *10*, 3382.
[38] G. H. Ryu, A. France-Lanord, Y. Wen, S. Zhou, J. C. Grossman, J. H. Warner, *ACS Nano* **2018**, *12*, 11638.
[39] F. Reale, P. Palczynski, I. Amit, G. F. Jones, J. D. Mehew, A. Bacon, N. Ni, P. C. Sherrell, S. Agnoli, M. F. Craciun, S. Russo, C. Mattevi, *Sci. Rep.* **2017**, *7*, 14911.
[40] T. Peters, C. Haake, J. Hopster, V. Sokolovsky, A. Wucher, M. Schleberger, *Nucl. Instrum. Methods Phys. Res., Sect. B* **2009**, *267*, 687.
[41] R. Kozubek, M. Tripathi, M. Ghorbani-Asl, S. Kretschmer, L. Madauβ, E. Pollmann, M. O'Brien, N. McEvoy, U. Ludacka, T. Susi, G. S. Duesberg, R. A. Wilhelm, A. V. Krasheninnikov, J. Kotakoski, M. Schleberger, *J. Phys. Chem. Lett.* **2019**, *10*, 904.